CrossMark

Shape controlled synthesis of rod-like Co_3O_4 nanostructures as high-performance electrodes for supercapacitor applications

V. Venkatachalam[1] · A. Alsalme[2] · A. Alswieleh[2] · R. Jayavel[1]

Abstract

Hydrothermal synthesis of Co_3O_4 nanorod electro-active material has been reported. The obtained Co_3O_4 material displays the cubic structure with 1D rod-like architecture. FT-IR and Raman spectral analyses have been carried out to confirm the functional groups and phase formation of Co_3O_4 electro-active material. Thermal stability of the as-prepared electro-active material has been studied by TG/DTA analysis. The electrochemical properties of the modified Co_3O_4 electrode have been analyzed by CV, CP and EIS using three electrode systems. The modified Co_3O_4 electrode exhibits the higher specific capacitance of 655 F g^{-1} at a current density of 0.5 A g^{-1} in 1 M KOH electrolyte. The high capacitance performance of the modified Co_3O_4 electrode was attributed to the highly crystalline rod-like structure. The Co_3O_4 electrode exhibits the excellent supercapacitive behaviour with better cyclic stability and high rate capacitive retention. The modified electrode reveals the Faradic behaviour, which is attributed to the redox contribution of Co(OH)/CoOOH (or) $Co^{2+} \leftrightarrow Co^{3+} \leftrightarrow Co^{4+}$ in alkaline medium that makes this material as a potential electrode for charge storage applications in supercapacitors.

1 Introduction

In recent years, energy crisis is one of the most important problems, which needs to be solved through search for high power and energy, low-cost and environmentally friendly energy storage technologies. Among varies energy storage technologies, supercapacitors and Li-ion batteries (LIBs) are widely used. Supercapacitors have been very attractive due to their primary advantages of high charge–discharge, excellent reversibility, long cycle life, high power and energy density as compared to normal battery and conventional capacitor. Supercapacitors are used in many devices such as, mobile phones, electric and hybrid vehicles, airbags, digital cameras, solar cell power storage, memory backup system and pulse laser [1–3].

Recently, the development of high performance nanostructured electro-active material is of great interest for supercapacitor, to achieve better electrochemical

performance with higher surface energy, strong surface activity and more electro-active sites than conventional bulk material. This leads to high utilization and results in superior energy storage performances [4]. In addition, the intrinsic inner porous structures of nanomaterials allow electrolyte infiltration and the reduced dimensions of particle size can shorten the transport and diffusion path lengths of electrolyte ions. The larger surface area allows higher current density during charging and discharging process [5]. Metal oxides are promising electro-active materials to achieve a higher performance. Among various metal oxides, Co_3O_4 is found to be one of the best alternate electro-active materials to MnO_2 [6], NiO [7] and CuO [8], due to its higher surface area, high redox activity, controllable size and shape, low cost, environmentally friendly and great reversibility.

The theoretical specific capacitance value of Co_3O_4 electrode material is reported to be 3560 F g^{-1} and the supercapacitance phenomenon is directly associated with surface properties; any change in the surface morphology of electro-active material greatly influences its electrochemical performance. The development of metal oxides with unique morphologies and structures have attracted great research interests in energy storage applications [9]. However, the one-dimension nanostructures have been extensively studied for their excellent physical and chemical properties. They provide large specific area, resulting in high utilization of

✉ R. Jayavel
rjvel@annauniv.edu

1   Centre for Nanoscience and Technology, Anna University, Chennai, Tamil Nadu 600 025, India

2   Department of Chemistry, College of Science, King Saud University, P.O. Box 2455, Riyadh, Riyadh 11451, Saudi Arabia

active materials. These materials are used as promising electrode materials for both supercapacitors and LIBs applications. Many efforts have been made to develop effective approaches to synthesize Co_3O_4 structures with different morphologies such as, nanosheets [10], ultra-layered Co_3O_4 [11], nanorod [12], broom-like Co_3O_4 [13], nanowire [14], conch-like [15], mushroom-like [16]. The electrochemical performance of the materials varies with morphology.

The hydrothermal method is widely used to synthesize nanostructured materials, because of the easy control of size, morphology, crystal structure and also the reaction temperatures are comparatively lower than the other methods [17]. In this paper, we aimed at developing the cobalt oxide nanostructured electrodes for supercapacitor through a facile hydrothermal process and explored the structural evolution and the formation mechanism. The electrochemical characterization demonstrates that the unique electrochemical properties of Co_3O_4 electrode are very much suitable for supercapacitor applications.

2 Experimental

2.1 Materials synthesis

In a typical Co_3O_4 nanorod synthesis process, 2 mol of cobalt chloride ($CoCl_2 \cdot 6H_2O$) was dissolved in 30 mL of distilled water along with 5 mol of urea [$CO(NH_2)_2$] dissolved in 10 mL of distilled water with stirring for about to 10 min. Subsequently, the two solutions were mixed at room temperature to form a homogeneous solution. After that, the mixture was transferred to 50 mL Teflon-liner autoclave for hydrothermal reaction at 120 °C for 12 h. Then, the autoclave was cooled to room temperature and the resulting product was collected by centrifugation after five times ultra-sonication process. The obtained product was washed several times with distilled water and ethanol for further purification and the dried product was calcined at 300 °C for 5 h.

2.2 Characterization of Co_3O_4 material

Structural analysis was carried out by powder X-ray diffraction (PXRD) analysis using Rigaku Mini Flex II-C system with CuKα ($\lambda = 1.54056$ Å) radiation at a scanning rate of $1°$/min. The morphology of the material was examined through high resolution transmission electron microscopy (HR-TEM) with Hitachi H7650 microscope. Thermal analysis was carried out using TGA [exstar S(II) TG/DTA 6300]. FT-IR study was performed using a Perkin Elmer spectrometer with KBr pellet-based samples in the frequency range from 4000 to 400 cm^{-1}. Raman spectrum was recorded in the

spectral range from 100 to 1000 cm^{-1} using Horiba Jobin-Yuon spectrometer.

2.3 Electrode material preparation and electrochemical measurements

The working electrodes were prepared by mixing the electro-active Co_3O_4, activated carbon, and polyvinylidene difluoride in a weight ratio of 8:1:1 and one drop of 1-methyl-2-pyrrolidinone was added to make the mixture more homogeneous. This slurry was coated onto a nickel foil. The electrochemical properties of the modified Co_3O_4 electrode were characterized by cyclic voltammetric (CV), chronopotentiometry (CP) and electrochemical impedance spectroscopy (EIS) analysis. All measurements were carried out in a conventional three-electrode cell in which platinum wire was used as the counter electrode, Ag/AgCl as the reference electrode and Co_3O_4 coated nickel foil as the working electrode. Cyclic voltammograms were recorded within a potential range between 0.0 and 0.45 V (vs. Ag/AgCl) for various scan rates ranging from 5 to 100 mV s^{-1} using Biologic VMP3 electrochemical workstation. The charge/discharge test was carried out using chronopotentiometry for different constant applied current values between 0.0 and 0.45 V (vs. Ag/AgCl). The electrochemical impedance spectrum was also recorded in the frequency range from 1 Hz to 1 MHz.

3 Results and discussion

3.1 X-ray diffraction analysis

The formation of FCC type Co_3O_4 with space group *Fd3m* was confirmed by powder X-ray diffraction (PXRD) pattern. Figure 1a displays the diffraction peaks, which could be indexed to crystalline cubic phase of Co_3O_4 with consistent standard JCPDS (Card file No. 65-3103). No impurity peaks were observed in the XRD pattern, which clearly demonstrates the high purity of the sample. The EDX spectrum of the Co_3O_4 electro-active material is presented in Fig. 1b, which reveals the presence of Co and O and it designates the elemental composition of Co_3O_4 with appropriate molar concentration.

3.2 TG/DTA analysis

Figure 2 shows the TG/DTA curve of the as-prepared Co_3O_4 electro-active material. The weight loss occurred in a three step process. The first weight loss of 4.84% was observed in the temperature range from 30 to 130 °C, which is attributed to the evaporation of physically absorbed water. The second weight loss of 31.42% was observed between 130 and 530 °C. It was inferred that the

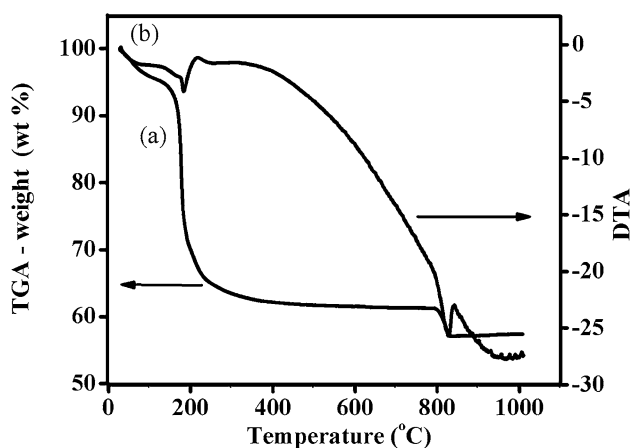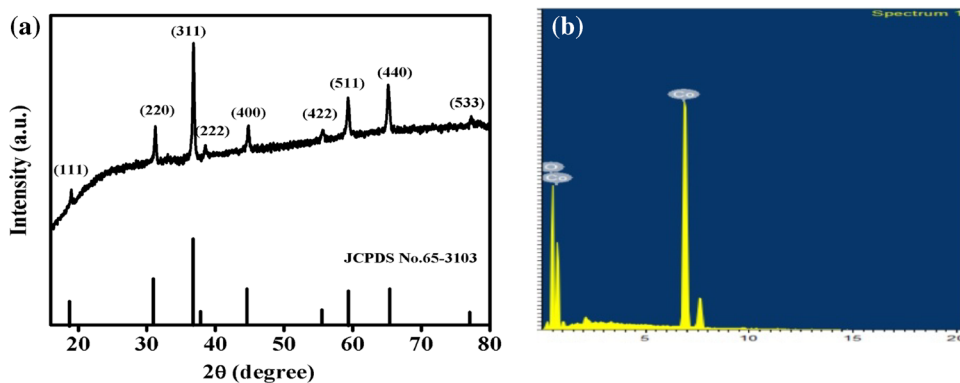**Fig. 1** **a** Powder XRD pattern and **b** EDX spectrum of Co_3O_4 electro-active material
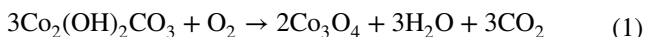

Fig. 2 *a* TGA and *b* DTA curves of as-prepared Co_3O_4 electro-active material

Fig. 3 FT-IR spectrum of prepared Co_3O_4 nanostructured electro-active material

thermal decomposition takes place leading to the formation of Co_3O_4 in this region. This value agrees well with the theoretical mass loss of 36.8%, corresponding to the following reaction. No change was observed in TG/DTA curves after 250 °C [18],

$$3Co_2(OH)_2CO_3 + O_2 \rightarrow 2Co_3O_4 + 3H_2O + 3CO_2 \quad (1)$$

When the temperature is increased above 250 °C, the TG curve becomes flat indicating that no phase transformation occurs and further heating could make the structure of the products more crystalline [19]. In Fig. 2b, a small endothermic peak was observed in the temperature range between 130 and 530 °C due to the oxidation of small amount of $Co(OH)_2$ contained in the Co_3O_4 sample. The endothermic peak at 820 °C supports the crystallinity with phase purity [20]. This endothermic reaction is due to the decomposition of the Co_3O_4 sample as given bellow,

$$2Co_3O_4 \rightarrow 6CoO + O_2 \quad (2)$$

In this work, the heat treatment temperature for the cobalt oxide was fixed at 300 °C according to the TGA result.

3.3 FT-IR analysis

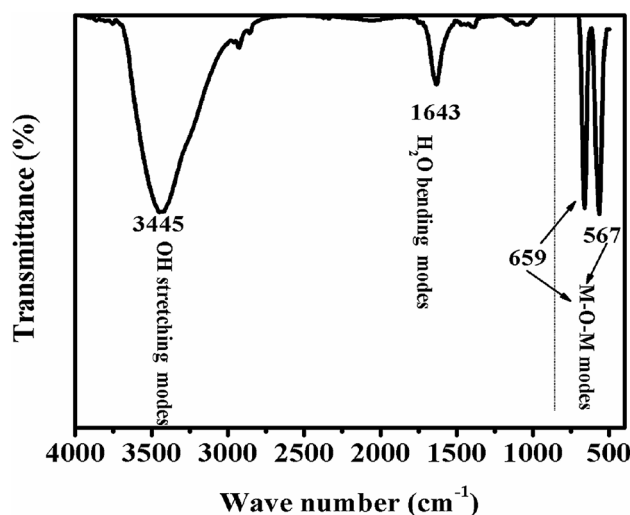The formation of the spinel Co_3O_4 sample was further supported by FT-IR spectrum as shown in Fig. 3. The sharp peaks at 567 and 659 cm^{-1} are assigned to the OB_3 (B represents Co^{3+} in an octahedral site) and the ABO (A represents the Co^{2+} in a tetrahedral site) vibrations in the spinel lattice, respectively [21]. The broadband at 3445 cm^{-1} could be attributed to the O–H stretching vibration of H_2O absorbed by the sample and the surface O–H. The band at 1643 cm^{-1} is associated with the H_2O molecules.

3.4 Raman spectroscopy analysis

The Raman spectrum of the synthesized Co_3O_4 sample is shown in Fig. 4. The Co_3O_4 crystallizes in the normal spinel structure, $Co^{2+}(Co^{3+})_2O_4^{2-}$ with Co^{2+} and Co^{3+} located at the tetrahedral and octahedral sites [22]. The five distinguishable Raman peaks are located at 194, 479, 519, 614, and 686 cm^{-1}, respectively, in which the major three
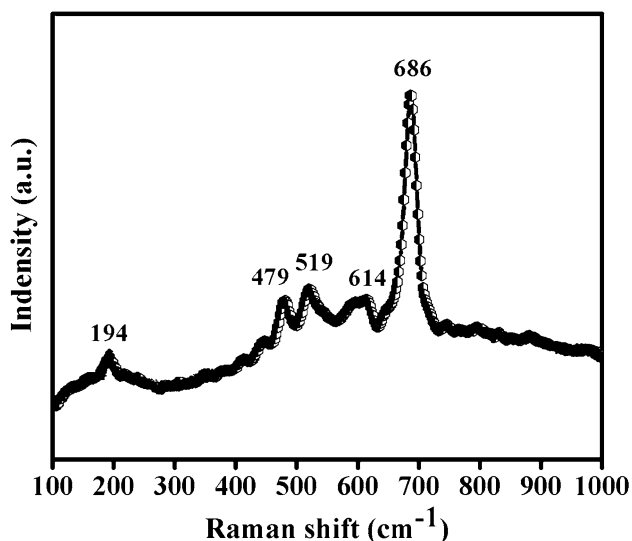
Fig. 4 The Raman spectrum of prepared Co_3O_4 nanostructured electro-active material

distinguishable Raman peaks located at 479 (E_g), 519 (F_{2g}) and 686 (A_{1g}) cm^{-1} were assigned to the Raman active modes of Co_3O_4 [23].
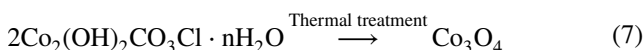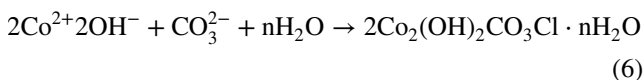
3.5 Morphological studies

The morphology of Co_3O_4 sample was studied by HR-TEM. Figure 5 shows the Co_3O_4 rod-like nanostructure. The SAED pattern for the Co_3O_4 material displays the regular diffraction dots. Hydrothermal condition is an advantage that improves the crystallization and control over the rod-like structure. In aqueous condition, decomposition and successive hydrolyzation of urea aqueous condition at elevated temperature leads to in situ release of OH^- and CO_3^{2-} ions. The generation of OH^- and CO_3^{2-} initiates the precipitation of Co^{2+} ions in the solution to produce cobalt hydroxide carbonate species.

The homogeneous precipitation process, including slow hydrolysis rate of urea, controlled generation of OH^- ions and crystal growth processes occurred in the medium. Additionally, hydrothermal condition adds the advantage of better control over the structure and crystallization. The possible

Fig. 5 HR-TEM images and SAED pattern of prepared Co_3O_4 electro-active material
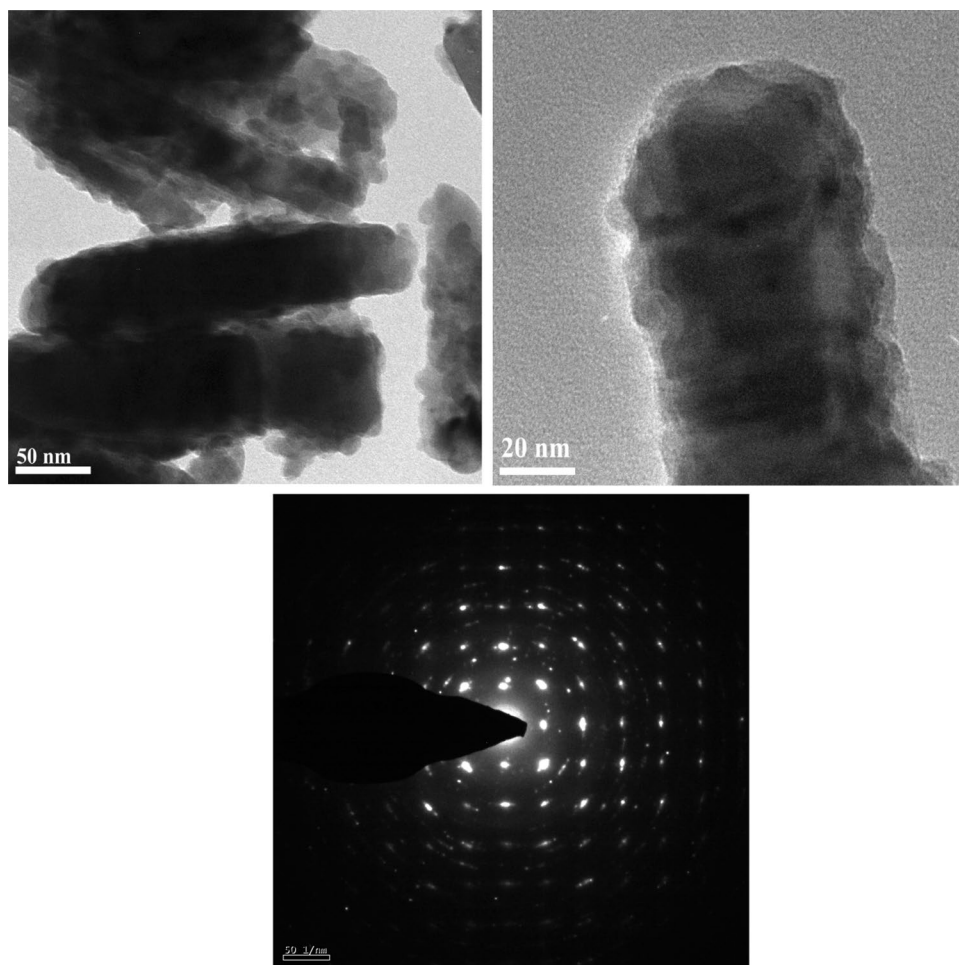
chemical reaction for the synthesis of Co_3O_4 nanorods can be expressed as,

$$NH_2CONH_2 \xrightarrow{Hydrolysis} NH_4^+ + NCO^- \quad (3)$$

$$NCO^- + 3H_2O \rightarrow HCO_3^- + NH_4^+OH^- \quad (4)$$

$$3HCO_3^- \rightarrow CO_3^{2-} + H^+ \quad (5)$$

$$2Co^{2+}2OH^- + CO_3^{2-} + nH_2O \rightarrow 2Co_2(OH)_2CO_3Cl \cdot nH_2O \quad (6)$$

$$2Co_2(OH)_2CO_3Cl \cdot nH_2O \xrightarrow{Thermal\ treatment} Co_3O_4 \quad (7)$$

The thermal treatment at elevated temperature supports the removal of CO_2 and H_2O species from the dried precursor sample and it transforms into Co_3O_4 phase by keeping its morphology intact. The Co_3O_4 nanorods can be formed through two steps. In the first step, the crystal structure of $2Co_2(OH)_2CO_3Cl \cdot nH_2O$ includes the Co–OH layers and counteranions between the Co–OH layers was formed through the hydrothermal route. In the second step, the resultant material was converted into Co_3O_4 nanorod during the calcination process, the Co–OH layers are converted into cobalt oxide nanoparticles through the dehydration and pyrolysis of counteranions into gases such as CO_2 and HCl.

3.6 Bet studies

Figure 6 shows the BET N_2 adsorption–desorption isotherm curves of the rod-like Co_3O_4 nanostructure. The BET surface area and pore size of the rod-like Co_3O_4 electrode material were calculated to be 38.6 $m^2\ g^{-1}$ and 3.45 nm respectively. Due to the higher surface area, the unique rod-like nanostructure provides the larger contact area between the electrolyte and electro-active material. Thus, it facilitates the ion transfer at the electrode/electrolyte interface. As a result, the synthesized rod-like Co_3O_4 is believed to be very effective in enhancing the electrochemical performance. Inset in Fig. 6 depicts the pore size distribution of the electro-active material.

3.7 Supercapacitive studies

The electrochemical properties of the modified Co_3O_4 electrode were evaluated by cyclic voltammetry analysis in 1 M KOH electrolyte. The CV curve of the modified Co_3O_4 electrode was analyzed in the potential range from 0 to 0.45 V (vs. Ag/AgCl) at a scan rate of 5 mV s^{-1} as shown in Fig. 7a. The pairs of redox peaks (A, B) can be clearly observed at low scan rate. The anodic peak at 0.34 V (positive current density) and cathodic peak at
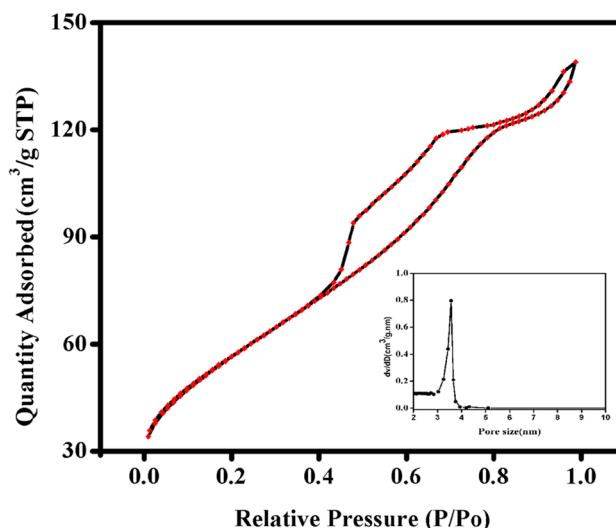

Fig. 6 BET N_2 adsorption–desorption analysis of the rod-likeCo_3O_4 nanostructures

0.23 and 0.28 V (negative current densities) are observed. These results reveal the oxidation of $Co^{2+} \rightarrow Co^{3+} \rightarrow Co^{4+}$ (during the charging process) and the reduction of $Co^{4+} \rightarrow Co^{3+} \rightarrow Co^{2+}$ (during the discharging process) of the Co_3O_4 material. The CV curves at different scan rates are shown in Fig. 7b. These results reveal that when the scan rate increases, the anodic peak (0.37 V) shifts towards the high potential range and the cathodic peak (0.25 V) moves towards the negative potential range, indicating the quasi-reversible feature of the redox couples [24, 25]. Within the potential window, the electrochemical reactions can be expressed as,

$$Co_3O_4 + OH^- + H_2O \leftrightarrow 3CoOOH + e^- \quad (8)$$

$$CoOOH + OH^- \leftrightarrow CoO_2 + H_2O + e^- \quad (9)$$
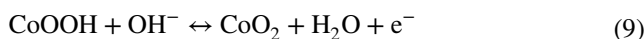
The CV curve reveals the Faradaic behavior for the charge storage characteristics of Co_3O_4 electrode. This process originates from the reversible redox reaction and continues in the presence of broad redox background, evidencing the sample's Faradaic behavior. The specific capacitance (Cs) of the modified Co_3O_4 electrode can be quantitatively evaluated using the following equation,

$$Cs = \frac{1}{v \times m(V_a - V_c)} \int_{V_a}^{V_c} IVdV \quad (10)$$

where Cs values were calculated graphically by integrating the area under the I–V curves and then dividing by the sweep rate v (mV s^{-1}), the mass of the material (m), and the potential window (Va to Vc) [26]. The calculated specific capacitance of the modified Co_3O_4 electrode was found to

Fig. 7 **a** CV curves of Co_3O_4 electrode material at 5 mV s^{-1} and **b** different scan rates of CV curves, **c** different current densities of charge–discharge curvesof Co_3O_4 electrode and **d** long cyclic stability studied at 3 A g^{-1} current density and inset figure illustrates the continuous cycles, **e** EIS spectrum of Co_3O_4 electrode and inset figure shows the equivalent circuit diagram and **f** specific capacitance values for different current densities and inset figure depicts the specific capacitance values for different scan rates and **g** Randles–Sevcik plot depicting the diffusion controlled process
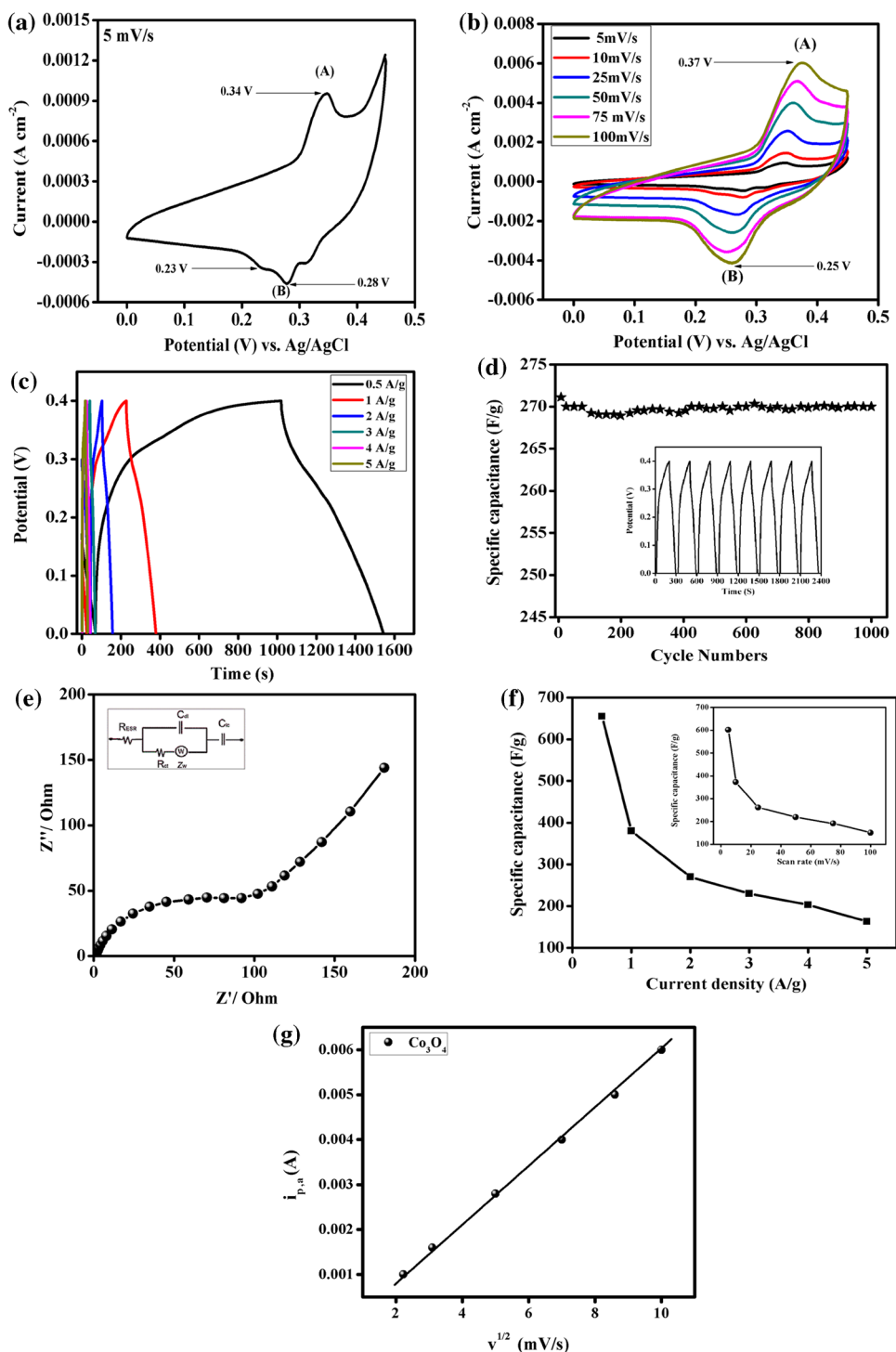
be 623 F g^{-1}. The modified Co_3O_4 electrode suggests the potential application in supercapcitors.

Figure 7c shows the galvanostatic charge–discharge analysis carried out in 1 M KOH electrolyte in the potential range between 0.0 and 0.45 V. The charge–discharge curves are slightly asymmetric with small internal resistance (IR) drop indicating the quasi-reversible kinetic feature of the

modified Co_3O_4 electrode. This demonstrates the typical Faradaic behavior, which could be caused by the charge transfer redox reaction (or) electrochemical adsorption–desorption process at the electrode and electrolyte interface [27, 28], which is in good agreement with the CV results. The linear charge–discharge curves validate the dominant Faradaic behavior of the electrode, which means that the capacitance

mainly comes from Faradaic reactions (or) redox reactions. The charge–discharge profile is divided into two parts, (i) a resistive component arising from the sudden voltage drop representing the voltage change attributed to the internal resistance and (ii) a capacitive component correlated to the voltage change due to changes in energy within the capacitor [29, 30]. The specific capacitance of the Co_3O_4 electrode material was calculated by using the following equation,

$$Cs = \frac{I \times t_d}{m \times \nabla V} \tag{11}$$

where I is the constant current applied, Δt is the discharge time, m is the mass of the material loaded and ΔV is the potential difference (0.4 V). The highest specific capacitance value of 655 F g^{-1} was obtained at a current density of 0.5 A g^{-1}. Due to the low Ohmic drop, inner active sites of the electrode can be fully accessed at low current densities. Hence, the highest specific capacitance value was achieved for Co_3O_4 electrode material. The observed specific capacitance values for the Co_3O_4 electrode is higher than the previous reports. Deng et al. reported cobalt oxides nanoparticels with the maximum specific capacitance value of 285.7 F g^{-1} at a current density of 4 A g^{-1} [31]. Co_3O_4 nano flakes were reported with specific capacitance value of 598.9 F g^{-1} at a current density of 6.25 A g^{-1} [32]. Mingjun Jing et al. reported the Co_3O_4 flakes with the maximum specific capacitance value of about 583 F g^{-1} at a current density of 1 A g^{-1} [33]. Co_3O_4 nano fibers were reported with the maximum specific capacitance value of 407 F g^{-1} at a scan rate of 5 mV s^{-1} [34]. Controllable synthesis of mesoporous Co_3O_4 nano flake array has been reported by Xiao et al. with a specific capacitance of 450 F g^{-1} at a current density of 1 A g^{-1} [35]. Zhao et al. reported the carbon supported cobalt oxide nanoparticles with specific capacitance value of 524.8 F g^{-1} [36]. Cobalt hydroxide was reported with a specific capacitance value of 358 F g^{-1} at a current density of 0.5 A g^{-1} [37]. Multi-shelled Co_3O_4 hollow microspheres exhibit the specific capacitance value of 394.4 F g^{-1} at a current density of 2 A g^{-1} [38]. The stability and reversibility are also important for electrochemical superpcapacitor applications. Figure 7d illustrates the stability characteristics of the modified Co_3O_4 electrode as a function of cycle number obtained from the chronopotentiometry at a current density of 3 A g^{-1} within the potential window of 0–0.45 V. The Columbic efficiency of the Co_3O_4 electrode was calculated using the relation,

$$\eta = \left(\frac{t_d}{t_c}\right) \times 100 \tag{12}$$

where η is the Columbic efficiency, t_d and t_c are the discharge time and charging time derived from charge–discharge curves. The capacitance of the electrode after 1000 cycles remains with the Columbic efficiency of 82.7%, which indicates the reasonable stability characteristics for supercapacitor application.

The electrochemical impedance spectroscopy studies were carried out for further understanding the capacitive behavior of modified Co_3O_4 electrode. Figure 7e shows the electrochemical impedance spectrum of Co_3O_4 electrode and inset reveals the equivalent circuit of modified electrode material. The Nyquist plot for the Co_3O_4 electrode measured in the frequency range from 1 Hz to 1 MHz exhibits a semicircle at high frequency region and lower slope in the medium frequency region. The electrochemical impedance spectrum was composed of three distinct regions. In the first region, the intercept on the real axis in the high frequency range provides the equivalent series resistance (ESR) and solution resistance (Rs), which includes the inherent bulk resistance of electrolyte, electro-active material and contact resistance at the interface between electrolyte and electrode. In the second region, the charge transfer resistance (Rct), which results from the diffusion of electrons, can be calculated from the diameter of semicircle in the high frequency range. The third region, Warburg resistance, which describes the diffusion of redox species in the electrolyte, can be reflected from the slope of the EIS curve in the low frequency range. This reveals that the Co_3O_4 electrode is a potentially active material for the supercapacitor applications [39, 40].

Figure 7f shows the plot between specific capacitance and various current densities. The highest specific capacitance value of 655 F g^{-1} was achieved at a current density of 0.5 A g^{-1}. Decrease in the capacitance value with increasing current density was due to the slow rate of redox reactions. These data show that Co_3O_4 electrode can act as an electro-active material for supercapcitors because of their ability to provide higher specific capacitance. The structural advantages ensure sufficient electrons and OH$^-$ ions to make contact with nearly entire surface of each Co_3O_4 nanorod for Faradaic reactions towards energy storage at high rates and enhance the electrochemical utilization of electro-active material. Inset in Fig. 7f shows the specific capacitance obtained from CV results. Figure 7g shows the Randles–Sevcik plot, anodic peak current (i_p, a) versus square root of scan rate ($v^{1/2}$). Linear relationship between them indicates the diffusion controlled rate kinetics of the electrode process. As the scan rate increases in the CV curves the anodic and cathodic peaks shift to the left and right respectively for cobalt oxide due to the polarization resistance.

4 Conclusion

The shape controlled cobalt oxide nanorods were prepared by hydrothermal method. The spinel structure of cobalt oxide without any secondary phase formation was confirmed

by XRD analysis. The thermal stability and decomposition of the prepared material were studied by TG/DTA analysis. The HR-TEM images showed the rod-likemorphology of Co_3O_4 electrode. The electrochemical properties of the modified Co_3O_4 electrode revealed the enhanced supercapacitor performance. The current density, reversibility, Columbic efficiency and capacitance retention of the electrode material demonstrated the good electrochemical performances. Based on the above results, the modified Co_3O_4 electrode material could be a promising and potential candidate for supercapacitor applications.

References

1. J.L. Liu, L.Z. Fan, X. Qu, Low temperature hydrothermal synthesis of nano-sized manganese oxide for supercapacitors. Eectrochim. Acta **66**, 302–305 (2012)
2. V. Venkatachalam, A. Alsalme, A. Alghamdi, R. Jayavel, High performance electrochemical capacitor based on $MnCo_2O_4$ nanostructured electrode. J Electroanal. Chem. **756**, 94–100 (2015)
3. Y. Zhang, J. Li, F. Kang, F. Gao, X. Wang, Fabrication and electrochemical characterization of two-dimensional ordered nanoporous manganese oxide for supercapacitor applications. Int. J. Hydrog. Energy **37**, 860–866 (2012)
4. Y. Xiao, A. Zhang, S. Liu, J. Zhao, S. Fang, D. Jia, F. Li, Freestanding and porous hierarchical nanoarchitectures constructed with cobalt cobaltite nanowalls for supercapacitors with high specific capacitances. J. Power Sources **219**, 140–146 (2012)
5. S. Chen, W.Xing, J. Duan, X. Hu, S.Z. Qiao, Nanostructured morphology control for efficient supercapacitor electrodes. J. Mater. Chem. A **1**, 2941–2954 (2013)
6. Y.F. Yuan, Y.B. Pei, S.Y. Guo, J. Fang, J.L. Yang, Sparse MnO_2 nanowires clusters for high-performance supercapacitors. Mater. Lett. **73**, 194–197 (2012)
7. S. Vijayakumar, S.Nagamuthu, G. Muralidharan, Supercapacitor studies on NiO nanoflakes synthesized through a microwave route. ACS Appl. Mater. Interfaces **5**, 2188–2196 (2013)
8. G. Wang, J. Huang, S. Chen, Y. Gao, D. Cao, Preparation and supercapacitance of CuO nanosheet arrays grown on nickel foam. J. Power Sources **196**, 5756–5760 (2011)
9. Y. Gao, S. Chen, D. Cao, G. Wang, J. Yin, Electrochemical capacitance of Co_3O_4 nanowire arrays supported on nickel foam. J. Power Sources **195**, 1757–1760 (2010)
10. K. Qiu, Y. Lu, J. Cheng, H. Yan, X. Hou, D. Zhang, M. Lu, X. Liu, Y. Luo, Ultrathin mesoporous Co_3O_4 nanosheets on Ni foam for high-performance supercapacitors. Electrochim. Acta **157**, 62–68 (2015)
11. S.K. Meher, G.R. Rao, Ultralayered Co_3O_4 for high-performance supercapacitor applications. J. Phys. Chem. C **115**, 15646–15654 (2011)
12. L. Wang, B. Liu, S. Ran, H. Huang, X. Wang, B. Liang, D. Chen, G. Shen, Nanorod-assembled Co_3O_4 hexapods with enhanced electrochemical performance for lithium-ion batteries. J. Mater. Chem. **22**, 23541–23547 (2012)
13. W. Liu, L. Xu, D. Jiang, J. Qian, Q. Liu, X. Yang, K. Wang, Reactable ionic liquid assisted preparation of porous Co_3O_4 nanostructures with enhanced supercapacitive performance. CrystEngComm. **16**, 2395–2403 (2014)
14. B. Vidyadharan, R.A. Aziz, I.I. .Misnon, G.M. Anil Kumar, J. Ismail, M.M. Yusoff, R. Jose, High energy and power density asymmetric supercapacitors using electrospun cobalt oxide nanowire anode. J. Power Sources **270**, 526–535 (2014)
15. K. Qiu, H. Yan, D. Zhang, Y. Lu, J. Cheng, W. Zhao, C. Wang, Y. Zhang, X. Liu, C. Cheng, Y. Luo, Hierarchical 3D mesoporous conch-like Co_3O_4 nanostructure arrays for high-performance supercapacitors. Electrochim. Acta **141**, 248–254 (2014)
16. F. Luo, J. Li, Y. Lei, W. Yang, H. Yuan, D. Xiao, Three-dimensional enoki mushroom-like Co_3O_4 hierarchitectures constructed by one-dimension nanowires for high-performance supercapacitors. Electrochim. Acta **135**, 495–502 (2014)
17. Y.Q. Li, X.Y. Zhang, S.J. Liu, X.Y. Shi, H. Zhao, X. Zhang, G.F. Ge, C.D. Cai, X.L. Gu, J.P. Wang, L. Tu, One-dimension $MnCo_2O_4$ nanowire arrays for electrochemical energy storage. Electrochim. Acta **116**, 467–474 (2014)
18. H. Yang, Y. Hu, X. Zhang, G. Qiu, Mechanochemical synthesis of cobalt oxide nanoparticles. Mater. Lett. **58**, 387–389 (2004)
19. L.B. Kong, J.W. Lang, M. Liu, Y.C. Luo, L. Kang, Facile approach to prepare loose-packed cobalt hydroxide nano-flakes materials for electrochemical capacitors. J. Power Sources **194**, 1194–1201 (2009)
20. D. Xu, Y. Yang, H. Cheng, Y.Y. Li, K. Zhang, Integration of nano-Al with Co_3O_4 nanorods to realize high-exothermic core–shell nanoenergetic materials on a silicon substrate. Combust. Flame **159**, 2202–2209 (2012)
21. M. Aghazadeh, Electrochemical preparation and properties of nanostructured Co_3O_4 as supercapacitor material. J. Appl. Electrochem. **42**, 89–94 (2012)
22. V.G. Hadjiev, M.N. Iliev, I.V. Vergilov, The Raman spectra of Co_3O_4. J. Phys. C **21**, L199-L201 (1988)
23. J. Pal, P. Chauhan, Study of physical properties of cobalt oxide (Co_3O_4) nanocrystals. Mater. Charact. **61**, 575–579 (2010)
24. X. Qing, S. Liu, K. Huang, K. Lv, Y. Yang, Z. Lu, D. Fang, X. Liang, Facile synthesis of Co_3O_4 nanoflowers grown on Ni foam with superior electrochemical performance. Electrochim. Acta **56**, 4985–4991 (2011)
25. S. Palmas, F. Ferrara, A. Vacca, M. Mascia, A.M. Polcaro, Behavior of cobalt oxide electrodes during oxidative processes in alkaline medium. Electrochim. Acta **53**, 400–406 (2007)
26. V. Venkatachalam, A. Alsalme, A. AlsIwieleh, R. Jayavel, Double hydroxide mediated synthesis of nanostructured $ZnCo_2O_4$ as high performance electrode material for supercapacitor applications. Chem. Eng. J. **321**, 474–483 (2017)
27. Y.Q. Wu, X.Y. Chen, P.T. Ji, Q.Q. Zhou, Sol–gel approach for controllable synthesis and electrochemical properties of $NiCo_2O_4$ crystals as electrode materials for application in supercapacitors. Electrochim. Acta **56**, 7517–7522 (2011)
28. J. Chen, K. Huang, S. Liu, Insoluble metal hexacyanoferrates as supercapacitor electrodes. Electrochem. Commun. **10**, 1851–1855 (2008)
29. R. Ding, L. Qi, M. Jia, H. Wang, Facile and large-scale chemical synthesis of highly porous secondary submicron/micron-sized $NiCo_2O_4$ materials for high-performanceaqueous hybrid AC-$NiCo_2O_4$ electrochemical capacitors. Electrochim. Acta **107**, 494–502 (2013)
30. S.G. Kandalkar, J.L. Gunjakar, C.D. Lokhande, Preparation of cobalt oxide thin films and its use in supercapacitor application. Appl. Surf. Sci. **254**, 5540–5544 (2008)

31. J. Deng, L. Kang, G. Bai, Y. Li, P. Li, X. Liu, Y. Yang, F. Gao, W. Liang, Solution combustion synthesis of cobalt oxides (Co_3O_4 and Co_3O_4/CoO) nanoparticles as supercapacitor electrode materials. Electrochim. Acta **132**, 127–135 (2014)

32. S.H. Kazemi, A. Asghari, M.A. Kiani, High performance supercapacitors based on the electrodeposited Co_3O_4 nanoflakes on electro-etched carbon fibers. Electrochim. Acta **138**, 9–14 (2014)

33. M. Jing, Y. Yang, Y. Zhu, H. Hou, Z. Wu, X. Ji, An asymmetric ultracapacitorsutilizing $\alpha Co(OH)_2$/Co_3O_4 flakes assisted by electrochemically alternating voltage. Electrochim. Acta **141**, 234–240 (2014)

34. M.A. Subramania, K. Balakrishnan, Preparation of electrospun Co_3O_4 nanofibers as electrode material for high performance asymmetric supercapacitors. Electrochim. Acta **149**, 152–158 (2014)

35. A. Xiao, S. Zhou, C. Zuo, Y. Zhuan, X. Ding, Controllable synthesis of mesoporous Co_3O_4 nanoflake array and its application for supercapacitor. Mater. Res. Bull. **60**, 674–678 (2014)

36. C. Zhao, J. Li, W. Chen, Y. Yang, K. Chiang, N. Burke, Synthesis and electrochemical properties of ordered mesoporous carbon supported well-dispersed cobalt oxide nanoparticles for supercapacitor. Mater. Res. Bull. **64**, 55–60 (2015)

37. Y. Tang, Y. Liu, S. Yu, S. Mu, S. Xiao, Y. Zhao, F. Gao, Morphology controlled synthesis of monodisperse cobalt hydroxide for supercapacitor with high performance and long cycle life. J. Power Sources **256**, 160–169 (2014)

38. Y. Wang, A. Pan, Q. Zhu, Z. Nie, Y. Zhang, Y. Tang, S. Liang, G. Cao, Facile synthesis of nanorod-assembled multi-shelled Co_3O_4 hollow microspheres for high-performance supercapacitors. J. Power Sources. **272**, 107–112 (2014)

39. V. Venkatachalam, A. Alsalme, A. Alghamdi, R. Jayavel, Hexagonal-like $NiCo_2O_4$ nanostructure based high-performance supercapacitor electrodes. Ionics **23**, 977–984 (2017)

40. R.B. Rakhi, W. Chen, D. Cha, H.N. Alshareef, Substrate dependent self-organization of mesoporous cobalt oxide nanowires with remarkable pseudocapacitance. Nano Lett. **12**, 2559–2567 (2012)